Real-Time Myoprocessors for a Neural Controlled Powered Exoskeleton Arm

Ettore E. Cavallaro*, *Member, IEEE*, Jacob Rosen, *Member, IEEE*, Joel C. Perry, and Stephen Burns

***Abstract*—Exoskeleton robots are promising assistive/rehabilitative devices that can help people with force deficits or allow the recovery of patients who have suffered from pathologies such as stroke. The key component that allows the user to control the exoskeleton is the human machine interface (HMI). Setting the HMI at the neuro-muscular level may lead to seamless integration and intuitive control of the exoskeleton arm as a natural extension of the human body. At the core of the exoskeleton HMI there is a model of the human muscle, the "myoprocessor," running in real-time and in parallel to the physiological muscle, that predicts joint torques as a function of the joint kinematics and neural activation levels. This paper presents the development of myoprocessors for the upper limb based on the Hill phenomenological muscle model. Genetic algorithms are used to optimize the internal parameters of the myoprocessors utilizing an experimental database that provides inputs to the model and allows for performance assessment. The results indicate high correlation between joint moment predictions of the model and the measured data. Consequently, the myoprocessor seems an adequate model, sufficiently robust for further integration into the exoskeleton control system.**

***Index Terms*—Exoskeletons, genetic algorithms, muscle models.**

I. Introduction

INTEGRATING human and robot into a single system offers remarkable opportunities for creating a new generation of assistive technologies for both healthy and disabled people. Humans possess naturally developed algorithms for control of movement, but they are limited by their muscle strength. In addition, muscle weakness is the primary cause of disability for most people with neuromuscular diseases and injuries to the central nervous system. In contrast, robotic manipulators can perform tasks requiring large forces; however, their artificial control algorithms do not provide the flexibility and quality of performance that is naturally achievable by humans. It seems, therefore, that combining these two entities, the human and the robot, into one integrated system under the control of the human, may lead to a solution that will benefit from the advantages offered by each subsystem. In this scenario, the exoskeleton robot, serving as an assistive device, is worn by the human (orthotic) and functions as a human-amplifier. Its joints and links correspond to those of the human body, and its actuators share a portion of the external load with the operator.

Several generations of exoskeletons can be defined based on the level of the human machine interface (HMI) between the exoskeleton robot and the human operator: (I) kinematic [1], [2]; (II) dynamic [3], [4]; (III) neuromuscular, e.g., surface electromyography (sEMG) [5], [6]; (IV) brain, e.g., noninvasive electroencephalogram (EEG) or invasive action potential signal measured directly from the motor cortex [7].

The third generation utilizes the body's own neural command signals as one of the primary command signals of the exoskeleton. The main advantage of establishing the interface at the neuromuscular level is the ability to estimate the effects of muscle contractions even before these effects can be directly measured using other means (e.g., kinematic and dynamic interfaces). In fact, an electro-(chemical)-mechanical delay (EMD), inherently exists in the musculoskeletal system. This inherent time delay refers to the interval between the time when the neural system activates the muscular system and the time when the muscles and the associated soft tissues contract mechanically and generate moments around the joints. EMD values vary considerably depending on the muscle, the person, and the experimental technique used for the measurements and can be assumed to be in the range of 26–131 ms with values for some upper limb muscles in the middle-lower part of this interval [8]–[10]. If the EMD can be exploited in the control algorithm of the exoskeleton, a noninvasive and seamless integration between the human operator and the exoskeleton can be achieved in such a way that the device becomes a natural extension of the operator's own body.

The primary component of the third-generation exoskeleton that takes advantage of the EMD and sets the HMI at the neuromuscular level is the *myoprocessor*. A myoprocessor is a set of computational representations (models) of a human muscle predicting joint torques in real-time. During the EMD, the system gathers information regarding the physiological muscle's neural activation level based on processed EMG signals, the joint position, and angular velocity. This information is fed into the myoprocessor which in turn predicts the moment that will be developed by the physiological muscle relative to the joint. The predicted moment is fed into the exoskeleton system such that, by the time the physiological muscle contracts, the exoskeleton amplifies the joint moment by a preselected gain factor. Part of the time gained by using these predicted muscle moments is employed by the electromechanical subsystems of the powered exoskeleton to compensate for their own inherent reaction time.

Manuscript received November 30, 2005; revised May 6, 2006. This work was supported in part by the National Science Foundation (NSF) under Grant 0208468 "Neural Control of an Upper Limb Exoskeleton System," J. Rosen (PI). *Asterisk indicates corresponding author.*

*E. E. Cavallaro is with the Department of Electrical Engineering, University of Washington, Seattle WA, 98185, USA and also with the ARTS Lab, Scuola Superiore Sant'Anna, Piazza Martiri della Libertà, 33, 56127 Pisa, Italy (e-mail: cavallaro@sssup.it).

J. Rosen is with the Department of Electrical Engineering, University of Washington, Seattle WA, 98185, USA (e-mail: rosen@u.washington.edu).

J. C. Perry is with the Department of Mechanical Engineering, University of Washington, Seattle WA, 98185, USA (e-mail: jcperry@u.washington.edu).

S. Burns is with the Department of Rehabilitation Medicine, University of Washington, Seattle WA, 98185, USA (e-mail: spburns@u.washington.edu).

Digital Object Identifier 10.1109/TBME.2006.880883

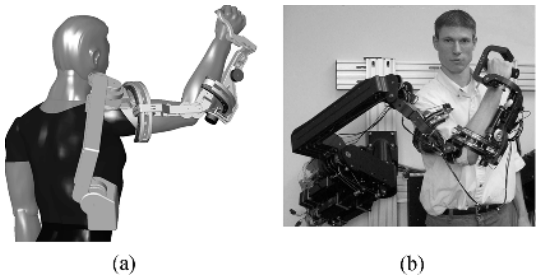

Fig. 1. A 7 DOF Exoskeleton arm: (a) CAD rendering of a 7 DOF upper limb powered exoskeleton – shoulder joint has 3 DOF, elbow joint has 1 DOF, wrist joint has 3 DOF; (b) Picture of the actual exoskeleton.

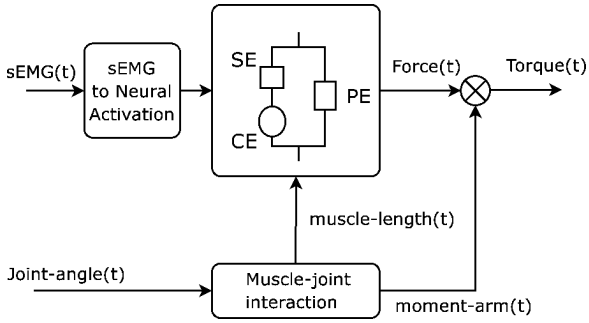

Fig. 2. Myoprocessor block diagram.

Although muscle has been the object of intense interest and study, and despite the enormous progress made in understanding its structure and function during the past few decades, the formulation of a completely satisfactory quantitative representation of contraction dynamics has been elusive. A great variety of muscle models have evolved over the years, differing in intended application, mathematical complexity, level of structure considered and fidelity to the biological facts (for review see [11]). According to this review, muscle models are classified as: 1) microscopic models; 2) distributed moment models; 3) macroscopic models; 4) fiber models. Hill-based models, viscoelestic models, and system models are subcategories of the macroscopic models class.

Previous research effort focused on developing and comparing the performance of two macroscopic muscle models including a Hill based muscle model and neural network model as part of a HMI for a single degree-of-freedom (DOF) powered exoskeleton [5], [6]. The current research effort is focused on developing a modular, myoprocessors-based, HMI for a 7-DOF upper limb powered exoskeleton (see Fig. 1). This HMI integrates Hill-based muscle models, kinematic models of the muscle lines of action, and the neural activity in the form of processed sEMG signals.

More specifically, this paper describes: 1) the development of real-time myoprocessors for the estimation of torques at the joints of the upper limb in dynamic conditions; 2) the development of a suitable strategy to adapt the parameters of the myoprocessors to a specific user; 3) the evaluation of the myoprocessors' performance by using experimental torque measurements during elbow and wrist flexion/extension movements.

II. Materials and Methods

The following sections define the fundamental elements of the myoprocessor, a genetic algorithm (GA) for adjusting myoprocessors' internal parameters and the experimental protocol to assess overall system performance.

A. The Myoprocessor

Each myoprocessor, as shown in Fig. 2, is composed of four modules: 1) a "neural activation module" which, by using sEMG signals, estimates the degree of neural activation of the muscle $a(t)$; 2) a "kinematics module" which, by using the joint angular positions and anatomical information, computes muscle length and moment arms; 3) a "Hill-based muscle model" which computes the force exerted by a muscle given the neural activation level and the muscle length (and lengthening/shortening velocity); 4) a "dynamics module" which evaluates muscle contribution to the joint moment as the product of muscle force and moment arm.

The Myoprocessor has been implemented in the Matlab/Simulink environment (MathWorks Inc.) utilizing the Real-time Workshop toolbox. Several routines have been written in C and integrated into the Simulink blocks in order to achieve real-time performance.

1) Neural Activation Module: By using the sEMG signal as input, this module estimates the level of the neural activation (NA) for each muscle under study. The NA is a normalized signal $a(t) \in [0,1]$, where $a = 1$ indicates a state of maximal voluntary activation and $a = 0$ represents no muscle activation. Commonly, the NA level is estimated by using the envelope of the rectified and normalized sEMG signal [12]–[15]. The module implemented in this study consists of a cascade of causal digital filters and nonlinear transformations: a) high-pass filter (cutoff frequency 20 Hz); b) notch filter (60 Hz); c) full wave rectification; d) low-pass filter (cutoff frequency 5 Hz); e) normalization with respect to the maximal isometric voluntary muscle activation levels; f) nonlinear scaling, defined by (1), where A determines the degree of nonlinearity [13]

$$a(t) = \frac{A^{u(t)} - 1}{A - 1}. \tag{1}$$

All the filters are Butterworth 4*th* order.

2) Kinematics Module: The kinematics module computes the length of the muscle and the moment arm for each DOF spanned by the muscle. In order to obtain these outputs, the angular positions of each joint spanned by the muscle, as well as anatomical information about the arm, are used. The muscle length and moment arms have a profound effect on the joint torque estimation [16], [17]. Several estimations of length and moment arms for the upper limb muscles are available [16], [18]–[20]. However, data are available only for a selected number of muscles and they are expressed as average values or as polynomial interpolations with respect to individual joint angles [17], [21]. Models accounting, to some extent, for the complex path of muscle from origin to insertion points have been developed [22]–[25]. These models allow the evaluation of muscle lengths and moment arms across multiple joints, and

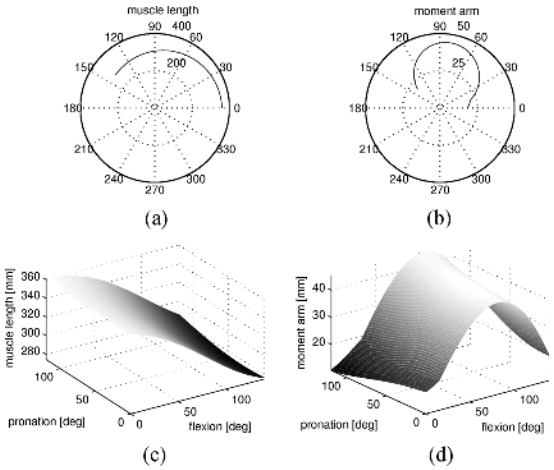

Fig. 3. The BSH length and moment arm as a function of angular position of joints: (a) the BSH length as a function of the elbow joint and the forearm angles; (b) the BSH moment arm as a function of the elbow joint and the forearm angles; (c) a polar plot of the BSH muscle length as a function of the elbow angle for a constant full supinated forearm; (d) a polar plot of the BSH muscle moment arm as a function of the elbow angle for a constant full supinated forearm.

for this reason have been chosen to represent the muscle-joints interaction in the present work.

In particular, in the work of Garner and Pandy [23]–[25], used as reference, each muscle is modeled as an elastic band attached to the origin and insertion points. The muscle can wrap around virtual objects (obstacles) that simulate other anatomical structures such as muscles, soft tissues, or bones, and its path can be constrained by fixed points (called via points). The obstacles are modeled as spheres, cylinders, or combination of these two basic primitives. The muscle path is then calculated as the shortest path from origin to insertion points given the obstacle constraints.

After calculating the muscle path, i.e., the muscle length, since the muscle line of action is also available, in the present work, the moment arms are evaluated by using the geometrical definition ($b_i = (\vec{r_i} \times \hat{F}) \cdot \hat{k_i}$), where b_i is the moment arm for the joint i, $\hat{k_i}$ is the direction of the joint axis of rotation, $\hat{F}$ is the unitary vector along the force direction and $\vec{r_i}$ is the distance vector from the rotation axis to the insertion point.

The present kinematic module included the following joints: glenohumeral, humero-ulnar flexion-extension, radio-ulnar pronation-supination, radio-carpal flexion-extension, and radio-carpal radial-ulnar deviation. As an example, Fig. 3 depicts the Biceps Brachii (short head) length and moment arm as a function of the elbow joint (flexion/extension) and forearm (pronation/supination) angles. During the validation phase, only the the humero-ulnar flexion-extension, and the radio-carpal flexion-extension joints were considered active, while the others were kept in fixed positions.

3) Hill-Based Muscle Model: This module predicts the force developed by the physiological muscle as a function of the estimated neural activity level, and of the calculated muscle's length and velocity. It is based on the phenomenological muscle model first described by Hill [26] and refined and used by many researchers in the last decades [14], [27]–[30].

The model includes three elements arranged on two branches. On one branch there are the passive serial element (SE) and the active contractile element (CE); on the other, there is the passive parallel element (PE), as shown in Fig. 2.

Given the mechanical arrangement of the PE, SE, and CE components, the two parallel branches of the model share the same displacement (2). In addition the two elements in series on the same branch share the same force (3). Finally, the total force generated by the muscle is the sum of the forces developed by each branch (4)

$$L_{\mathrm{PE}} = L_{\mathrm{CE}} + L_{\mathrm{SE}} \tag{2}$$

$$F_{\mathrm{SE}} = F_{\mathrm{CE}} \tag{3}$$

$$F_{tot} = F_{\mathrm{CE}} + F_{\mathrm{PE}} = F_{\mathrm{SE}} + F_{\mathrm{PE}} \tag{4}$$

where F is the force and L is the length of an element.

Given the passive nature of the PE and SE elements, the force generated by these two elements as a function of the displacement, is expressed by the same equation with different internal parameters (5)

$$F_{\mathrm{PE,SE}} = \left[\frac{F_{\max}}{e^S - 1}\right]\left[e^{((S/\Delta L_{\max})\Delta L)} - 1\right] \tag{5}$$

where $F_{\mathrm{PE,SE}}$ is the passive force generated by the PE or the SE element, ΔL is the change in length of the element with respect to the slack length, S is a shape parameter (related to the stiffness of the element), $F_{\max}$ is the maximal force exerted by the element for the maximum change in length $\Delta L_{\max}$.

The force F_{CE} generated by the CE element is a function of the neural activation a, of the normalized force-length function f_l, of the normalized force-velocity function f_v, and of a fixed parameter $F_{\mathrm{CE}_{\max}}$ defining the maximal force the element can generate [see (6)–(9)]

$$F_{\mathrm{CE}} = a \cdot f_l \cdot f_v \cdot F_{\mathrm{CE}_{\max}} \tag{6}$$

$$f_l = \exp\left(-0.5\left(\frac{\frac{\Delta L_{\mathrm{CE}}}{L_{\mathrm{CE}_0}} - \phi_m}{\phi_v}\right)^2\right) \tag{7}$$

$$f_v = \frac{0.1433}{0.1074 + \exp\left(-1.3\sinh\left(2.8\frac{V_{\mathrm{CE}}}{V_{\mathrm{CE}_0}} + 1.64\right)\right)} \tag{8}$$

$$V_{\mathrm{CE}_0} = 0.5(a+1)V_{\mathrm{CE}_{\max}}. \tag{9}$$

f_l is modeled as a Gaussian function (7) where ΔL_{CE} is the length change for the CE element and L_{CE_0} is the optimal fiber length; ϕ_m and ϕ_v are parameters affecting the mean value and variance of the Gaussian. The force-velocity equation is defined by (8) where V_{CE} is the CE velocity and V_{CE_0} is the maximal CE velocity when $F_{\mathrm{CE}} = 0$. V_{CE_0}, as shown in (9), can be expressed as a function of neural activation and $V_{\mathrm{CE}_{\max}}$, i.e., V_{CE_0} when the activation is maximum ($a = 1$). Moreover, the following relations hold for some of the parameters in the previous equations [16], [30]

$$V_{\mathrm{CE}_{\max}} = 2 \cdot L_{\mathrm{CE}_0} + 8 \cdot L_{\mathrm{CE}_0} \cdot \alpha \tag{10}$$

$$F_{\mathrm{PE}_{\max}} = 0.05 \cdot F_{\mathrm{CE}_{\max}} \tag{11}$$

$$\Delta_{\mathrm{PE}_{\max}} = L_{\max} - (L_{\mathrm{CE}_0} + L_{T_s}) \tag{12}$$

$$F_{\mathrm{SE}_{\max}} = 1.3 \cdot F_{\mathrm{CE}_{\max}} \tag{13}$$

$$\Delta_{\mathrm{SE}_{\max}} = 0.03 \cdot L_{T_s} \tag{14}$$

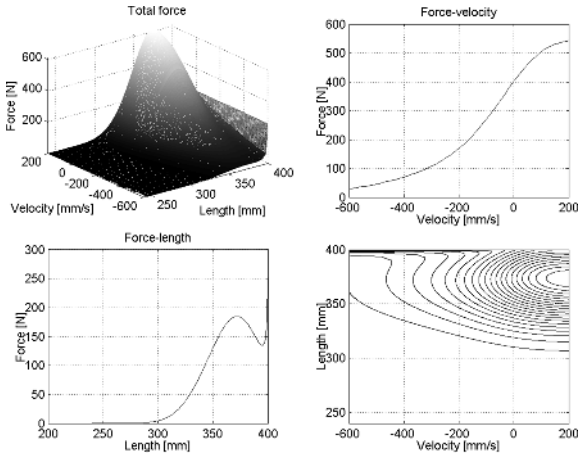

Fig. 4. Force as a function of velocity and muscle length for the BSH (nonoptimized parameters). Activation is held constant to 1. The two cross sections are for $\mathrm{L} = 360\ \mathrm{mm}, \mathrm{V} = -400\ \mathrm{mm/s}$. Velocity and length refer to the whole muscle+tendon structure.

where α is the percentage of fast fibers in a muscle, L_{T_s} is the tendon slack length (other symbols have been previously defined).

Fig. 4 shows an example of the force-length-velocity surface described by the previous equations for a maximal neural activation $a = 1$. As can be noted, there are infinite surfaces encapsulated underneath this surface for various activation levels. Essentially any point on and under this surface is a potential operational state for the muscle.

Given the length of the muscle (which is equal to the length of the PE element, L_{PE}) and the neural activation a, there are two main ways to compute the force generated by the muscle by using (5)–(9).

Equation (8) can be inverted to find V_{CE} as a function of $F_{\mathrm{SE}}/af_l F_{\mathrm{CE}_{\max}}$; then V_{CE} can be integrated to obtain L_{CE}. It is clear that when $a(t)$ approaches zero this method cannot be used.

Alternatively, (8) can be transformed into a nonlinear finite difference equation (15). This equation can be solved numerically and in real-time by using the bisection method

$$F_{\mathrm{SE}}(\Delta L_{\mathrm{CE}}[n]) = \frac{0.1433 \cdot a \cdot f_l \cdot (\Delta L_{\mathrm{CE}}[n]) \cdot F_{\mathrm{CE}_{\max}}}{0.1074 + \exp\left(-1.3 \sinh\left(2.8 \frac{\Delta L_{\mathrm{CE}}[n] - \Delta L_{\mathrm{CE}}[n-1]}{\Delta t \cdot V_{\mathrm{CE}_0}} + 1.64\right)\right)}. \quad (15)$$

4) Dynamics Model: The net moment developed in each joint is the sum of all the moments applied by agonist and antagonist muscles (16). The moment developed by each muscle (T_i) at a certain joint is computed by

$$\tau_{net} = \sum_i \tau_i \quad (16)$$

$$\tau_i = F_i \cdot b_i \quad (17)$$

where F_i is the force generated by a single muscle and b_i is the moment arm of the muscle for that specific joint.

B. Muscle Synergy – The Inverse Problem – Force/Torque Estimation With No sEMG Inputs

In the present work, 12 muscle bundles have been modeled, namely *Brachialis (BRA), Biceps Brachii long head (BLH), Biceps Brachii short head (BSH), Brachioradialis (BRD), Triceps Brachii long head (TLgH), Triceps Brachii medial head (TmH), Triceps Brachii lateral head (TLtH), Flexor Carpi Radialis (FCR), Extensor Carpi Radialis (ECR), Flexor Carpi radialis (FCU),* and *Extensor Carpi Ulnaris (ECU).*

However, the sEMG were recorded from 9 muscles only, due to anatomical limitations in accessing some muscles using noninvasive techniques. Several methods can be used to address this issue. In the present work, the following two techniques have been used.

- The neural activity of muscle bundles close together, measured by a single pair of electrodes, has been assumed to be the same except for a scaling factor. This approach was used to model the neural activation of the biceps BSHs and BLHs;
- The criterion of "maximum endurance of musculoskeletal function" introduced in [31] has been used for predicting load sharing of synergistic muscle groups.

Based on this criterion, muscles with a larger cross section will share higher force then muscles with small cross sections depending also on their moment arms. The predictions from this criterion are improved when the moment arms are allowed to vary with joint angular position [32], as in the present study.

The "maximum endurance of musculoskeletal function" criterion has been used to model the force and torque exerted by the Brachialis muscle. An equivalent two agonist model has been defined between the BRA and the BSH, BLH, and BRD lumped together. Then, the BRA force has been computed as follows:

$$F_{\mathrm{BRA}} = \left(\frac{b_{\mathrm{BRA}}}{b_\Sigma}\right)^{1/2} \left(\frac{F^{\max}_{\mathrm{BRA}}}{F^{\max}_\Sigma}\right)^{3/2} F_\Sigma \quad (18)$$

$$b_\Sigma = \frac{\tau_\Sigma}{F_\Sigma} \quad (19)$$

$$F_\Sigma = F_{\mathrm{BRD}} + F_{\mathrm{BSH}} + F_{\mathrm{BLH}} \quad (20)$$

$$\tau_\Sigma = \tau_{\mathrm{BRD}} + \tau_{\mathrm{BSH}} + \tau_{\mathrm{BLH}} \quad (21)$$

where F represent the force developed by a muscle, τ is the torque developed by a muscle for the humero-ulnar joint, b is the moment arm of each muscle, which varies according to angular position, and $F^{\max}$ is the maximum force that a muscle can exert.

C. Myoprocessor Parameters Optimization—Genetic Algorithms (GAs)

As previously defined, each muscle model has several internal parameters. To insure an optimal performance, these internal parameters have to be adjusted for each user. Two main types of variability can be identified: 1) variability due to the placement of electrodes; 2) variability due to anatomical and physiological differences between subjects.

The two sources of variability can be addressed by two different parameter optimization strategies. Type II variability (Intersubject) requires a global parameter optimization to be run

only once (or each time a major change takes place), in order to find the optimal set of parameters. Type I variability can be addressed with a faster optimization targeting only parameters of the sEMG to neural activation module. This latter optimization is used each time the user wears the exoskeleton. In this section a strategy for the global parameter optimization (type II) using a GA is described.

GAs are commonly used as optimization techniques because they can deal with very large search spaces, minimizing the risk of finding solutions that are only locally optimal [33], [34]. Their use for the optimization of Hill based muscle models has also been recently suggested [13].

GAs find an optimal solution by using simulated evolution processes. The optimal parameters search starts from an initial random population of "chromosomes," each of them representing a set of parameters of the various muscle models, and, thus, a potential solution. The "survival of the fittest" criterion and "genetic operators" are used to reach a final optimal population [35]. The degree of fitness of a certain set of parameters is evaluated by a problem-specific fitness function. In the present work the best "chromosome" is the one which minimizes the rms error between the torque estimated by the model and the torque estimated by a reference method. The GA implementation follows a stepwise process.

1) Encode the parameters of the problem into a chromosome. Choose an alphabet (such as binary or real numbers) for the genes and choose selection, mutation, crossover, and fitness functions (genetic operators).
2) Create the initial population of chromosomes and estimate, using a fitness function, the fitness degree of every chromosome.
3) Create an intermediate population, selecting elements from the previous population, using the selection function (a function that privileges individuals with a higher degree of fitness).
4) Create new individuals using crossover and mutation and insert them into the population which becomes the new population ("children" substitute "parents" so that population size is stable).
5) If there is an individual whose fitness function is above a desired threshold or a maximum number of generations is reached, terminate the evolution process, otherwise start again from Step 3.

Many parameters in the model can be optimized. Analytical estimation of the sensitivity of the model for the different parameters is not trivial, since the equations are nonlinear and, thus, sensitivity changes with the working point. For isometric conditions, some indications on the more significant parameters and on the optimization strategy to be used (muscle specific or only agonist/antagonist specific) are available [17], [36]. Given the complexity of the problem, no definitive guidance is available for the other loading conditions.

In this study, the chromosome has been designed with 121 "genes" (see Table I). Eleven parameters were selected for each of the 11 myoprocessors out of the twelve modeled (the modeling approach used for Brachialis does not require optimization of parameters).

The following parameters were optimized in this study.

TABLE I
GENES INSERTED IN THE CHROMOSOME FOR EACH MUSCLE. EACH GENE CORRESPONDS TO A PARAMETER OF THE MYOPROCESSOR EXCEPT FOR GENES MARKED WITH AN "*" WHERE THE GENE IS A SCALING FACTOR, I.E., THE OPTIMIZED PARAMETER IS OBTAINED BY MULTIPLYING THE GENE AND THE NOMINAL PARAMETER

Gene	Boundaries
A	[0.05, 1[
* L_{CE_0}	[0.8, 1.2]
* L_{T_s}	[0.8, 1.2]
* $F_{CE_{max}}$	[0.5, 1.5]
α	[0.25, 0.75]
*S_{PE}	[0.8, 1.2]
* S_{SE}	[0.8, 1.2]
O_b	[-5, 5] mm
G_b	[0, 1.2]
ϕ_m	[-0.1, 0.1]
ϕ_v	[0.09, 0.8]

- *sEMG to neural activation model*: nonlinear scaling factor (A)—the boundaries used for this value allowed the scaling to range from linearity to strong nonlinearity; there is no clear physiological range for this parameter;
- *kinematic model*: moment arm gain factor (G_b) and offset (O_b); these two values define the linear transformation of the moment arm in (22), where b is the moment arm and $\overline{b}$ is the average moment arm—the boundaries used for these two parameters allowed the optimization of the moment arms but they do not have physiological meaning

$$\tilde{b} = (b - \overline{b})G_b + \overline{b} + O_b. \tag{22}$$

- *Hill model*: optimal fiber length (L_{CE0}), maximum force ($F_{CE\,\max}$), and tendon slack length (L_{T_s})—the boundaries chosen for these parameters allowed their variation in the range $\pm 20\%$, $\pm 50\%$, and $\pm 20\%$, respectively, with respect to the nominal values (see Table II); the values presented in the literature for these parameters show a significant dispersion due to the different measurement conditions (measurements on cadaver, cryo-sections, male, female, old, young, etc.); the boundaries chosen allow for optimization still maintaining physiological significance; moreover, in the optimization routine, a constraint has been introduced in order to guarantee that $L_{\max} > L_{\mathrm{CE}_0} + L_{T_s}$; fraction of fast fibers (α)—this parameter has been constrained to vary between 25% and 75%; shape parameters (S_{PE}, S_{SE}) of the passive elements—these parameters can be adjusted in a $\pm 20\%$ interval around the nominal values of Table II; anyway it is difficult to determine a physiological range for them; ϕ_m and ϕ_v parameters of the force-length equation—these values are allowed to vary between the intervals shown in Table I, so that the qualitative shape of the force-length function is maintained.

Some of the nominal values of parameters for each myoprocessor are listed in Table II. The nominal values not listed in the tables are: $A = 1, O_b = 0, G_b = 1, \phi_m = 0.05$, and $\phi_v = 0.19$.

TABLE II
NOMINAL PARAMETERS FOR THE MYOPROCESSOR MODEL BASED ON [24] AND [30]

Muscle	L_{max} [cm]	L_{CE_0} [cm]	L_{T_s} [cm]	$F_{CE_{max}}$ [N]	α [%]	S_{PE}	S_{SE}
BSH	40.46	13.07	22.98	461.76	56	9	2.8
BLH	41.94	15.36	22.93	392.91	56	9	2.8
TLgH	40.29	15.24	19.05	1000	66	10	2.3
TMH	18.95	4.90	12.19	1000	66	10	2.3
TLtH	28.22	6.17	19.64	1000	66	10	2.3
BRD	35.35	27.03	6.04	101.58	75	9	2.6
BRA	13.01	10.28	1.75	853.90	38	9	3
FCR	34.78	5.10	27.08	368.41	58	6	3
FCU	33.62	3.98	27.14	560.7	57	6	3
ECRB	34.53	5.59	26.87	553.21	44	8	3
ECRL	38.33	8.96	26.80	2.68.42	50	8	3
ECU	33.68	3.56	28.18	256.27	45	8	3

D. Experimental Protocol and Preliminary Data Processing

The experimental protocol designed to test the myoprocessors included the recording of movements for two joints of the upper limb: elbow and wrist.

The flexion/extension movements of the elbow joint (0-145° range) was performed using the "Arm Curl" VR2 Cybex exercise machine (Cybex International, Inc) (Fig. 5). Each movement was repeated three times with three different loads (4.54, 6.80, and 9.07 Kg) moving at three angular velocities (average values of 1.8 ± 0.26, 1.4 ± 0.13, 0.7 ± 0.04 rad/s, that are further referred to as fast, medium and slow). The joint angle was measured by a potentiometer (Midori America Corp., Fullerton, CA) located on the Cybex machine. sEMG signals were collected using Silver-Silver Chloride surface electrodes (In Vivo Metric, Healdsburg, CA) from 28 individual right upper-limb, chest, and back muscles (Fig. 5). Electrodes were placed by following the recommendations in [37], [38] in order to achieve optimal signal detection. Maximal voluntary muscle activations were recorded during isometric contractions. The sEMG signals were amplified by using a custom system with eight Teledyne A0401 modules (Teledyne Inc., CA). Each EMG channel had a gain of 1 K, common mode rejection ratio 100 dB, a first-order high-pass filter with a cutoff frequency 0.5 Hz and a sixth-order anti-aliasing low-pass filter with a cutoff frequency of 500 Hz. The time constant introduced by these filters can be neglected, compared to the time constant introduced by software filter used in the Neural activation module that is of the order of 80 ms. The data were sampled at 1 KHz by a 14-bit analog-to-digital card (United Electronic Industries, Canton, MA) using the Matlab Real-time workshop toolbox (Mathworks Inc., Natick, MA).

The muscular torques at each joint have been estimated by using a model of the Cybex machine and the human arm dynamics [39] described by (23)–(25), where R is the radius of the pulley of the Cybex machine, m is the mass, θ is the angular position ($\theta = 0$ corresponds to the elbow fully extended), I is the lumped inertia of the Cybex machine and the human arm.

(a) (b)

Fig. 5. (a) Surface electrodes attached to the subject measuring EMG signals from 28 muscles simultaneously; (b) flexing and extending the elbow joint under different loads using CYBEX exercise machine while recording the joint position and muscle EMG signals.

τ_{fl} is the torque computed for flexion movements and τ_{ex} is the torque for extension movements

$$\tau_{fl} = R\left[mg + m\left(\theta\ddot{R} + 2\dot{R}\dot{\theta} + \ddot{\theta}R\right)\right] + I\ddot{\theta} \quad (23)$$

$$\tau_{ex} = -R\left[mg - m\left(\theta\ddot{R} + 2\dot{R}\dot{\theta} + \ddot{\theta}R\right)\right] + I\ddot{\theta} \quad (24)$$

$$R = R(\theta). \quad (25)$$

This mechanical modeling of the Cybex machine provides a reference joint torque to which the myoprocessor output is compared during parameter optimization and testing. There are possible sources of uncertainty (such as approximation of geometry, inertia, etc.) that cause an estimated uncertainty for joint torques in the range of 3 to 4 Nm (about 6%-8% of the maximal peak-to-peak measured torque).

The wrist exercises involved the use of free weights (four different loads: 0.45, 1.04, 1.41, and 2.06). Each movement was repeated three times. Wrist flexion movements were performed with the elbow flexed at 110 deg and the forearm fully supinated. Wrist extension movements were performed in the same condition but with the forearm fully pronated. The wrist position was measured by an electrogoniometer fixed to the forearm and the hand. The torques were estimated by using (26)–(27) where m is the free weight plus the hand weight, R is the distance from the joint axis to the center of mass of the hand and weight system, θ is the joint angle (positive values for flexion and negative for extension), and I is the inertia

$$\tau_{fl} = Rmg\cos(\theta) + I\ddot{\theta} \quad (26)$$

$$\tau_{ex} = -Rmg\cos(\theta) + I\ddot{\theta}. \quad (27)$$

An error analysis similar to the one performed for the elbow joint indicated that the uncertainty in the wrist reference torques is in the range of 0.05 to 0.1 Nm (about 3.5%–7% of the maximal peak-to-peak measured torque).

E. Performance Metrics

The model predictions were assessed with respect to the reference joint torques by using three criteria: maximum error (28), root mean squared error (29), and correlation coefficient (30). The root mean squared error was also used as a fitness function for the GA

$$E_{\max} = \max_i |\tau[i] - \tilde{\tau}[i]| \quad (28)$$

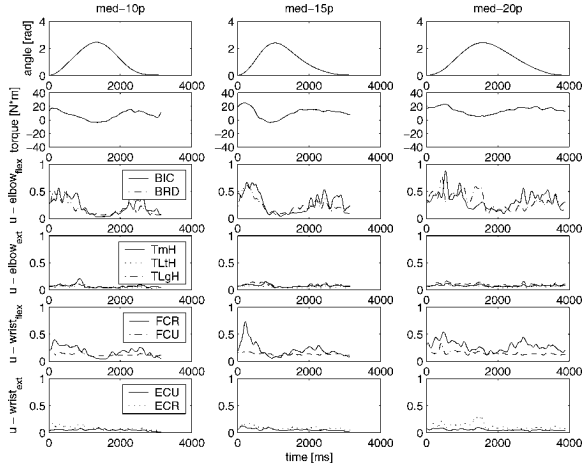

Fig. 6. Typical datasets recorded as part of the experimental protocol for various loading conditions during flexion/extension of the elbow joint.

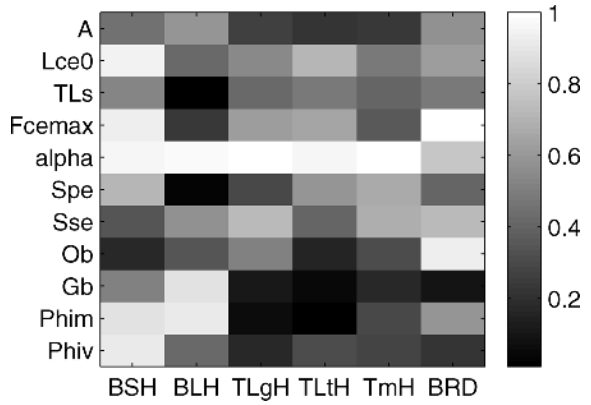

Fig. 7. Representation of myoprocessors parameters after optimization (elbow movements). Values are mapped in the range 0–1; see Table I for actual min and max values.

$$E_{\mathrm{rms}} = \sqrt{\frac{1}{N}\sum_{i=1}^{N}(\tau[i] - \tilde{\tau}[i])^2} \tag{29}$$

$$\rho = \frac{C_{\tau\tilde{\tau}}}{\sigma_\tau \sigma_{\tilde{\tau}}} \tag{30}$$

where τ represents the reference torque, $\tilde{\tau}$ is the torque computed by the model, and N is the number of sample points, $C_{\tau\tilde{\tau}}$ is the covariance coefficient, σ_τ and $\sigma_{\tilde{\tau}}$ are the standard deviations.

An additional parameter used to asses the performance of the myoprocessors is the percentage of time (η_s) the absolute error is below a specific threshold value (namely, $s = 4,6\ \mathrm{Nm}$ for the elbow and $s = 0.4, 0.6\ \mathrm{Nm}$ for the wrist)

$$\eta_s = \frac{\sum_{k=1}^{M} 1}{N} \quad (\forall k \mid |\tau[k]| \leq s). \tag{31}$$

III. Results

During the first phase of the experimental recordings, flexion and extension movements of the elbow were performed; in a second phase, recordings were done during flexion and extension movements of the wrist. An example of kinematics (joint angles), dynamics [joint torques, estimated by using (23)–(27)], and of the neural activation levels of some muscles as a function of time are depicted in Fig. 6.

The angular joint positions and the neural activation levels of the muscles were used as inputs to the myoprocessors. Some of the joint torques have been used as a reference to optimize the model parameters; the remaining torque estimations have been used to assess the myoprocessor predictions. More specifically, the myoprocessor parameters of the FCU, FCR, ECRB, ECRL, and ECU muscles have been optimized by using repetition #2, 1.04-Kg load, flexion, and repetition #2, 1.04-Kg load, extension movements (thus, 2 recordings have been used during optimization and 22 during testing). The myoprocessor parameters of the BRD, BLH, BSH, TmH, TLgH, and TLtH, muscles have been optimized on repetition #2, medium velocity, medium weight, flexion movement, and repetition #2, medium velocity, medium weight, extension movements (thus, 2 recordings have been used during optimization and 52 during testing).

As an example, the chromosome obtained after optimization on the elbow movements is shown in Fig. 7.

The performances of the myoprocessors during the test phase are summarized in Table III. The values presented refer to the metrics defined in (28)–(31). The results are averaged over the entire test dataset (test data have not been used for the model optimization).

Some typical joint torques predicted by the myoprocessors after parameter optimization are plotted in Fig. 8. More in detail, Fig. 8(a)-top represents a flexion movement of the elbow (repetition #3, fast movement, 6.8 Kg); Fig. 8(a)-bottom represents an extension movement (repetition #3, medium velocity, 6.8 Kg). Each plot includes three torques: 1) the myoprocessor predictions with nominal model parameters (nonoptimized); 2) the reference torque as computed by using (23)–(27); 3) the myoprocessor predictions with optimized parameters. Examples for flexion movement and an extension movement of the wrist are presented in Fig. 8(b). Top plot is a flexion movement—repetition #3, 1.04 Kg; bottom plot is an extension movement—repetition #3, 1.04 Kg. Also in this case each plot includes three torques: 1) the myoprocessor predictions with nominal model parameters (nonoptimized); 2) the reference torque as computed by using (23)–(27); 3) the myoprocessor predictions with optimized parameters.

One important characteristic of the myoprocessors described in the present work is their ability to work in real-time. Given a specific computational power, there is a delicate balance between the complexity and number of the myoprocessors and the capability of the hardware system to perform in real-time. The task execution time (TET) of the myoprocessors system as a function of the number of muscles modeled is presented in Fig. 9. The TET was estimated simulating a flexion movement of the elbow, with angular position described by a saw-tooth spanning the 0°–145° range of motion; other joints are held in a neutral position; neural input was held constant at an activation level of 0.5 (50% of the maximal voluntary activation level). The saw-tooth had a period of 1 second. Max, min, and averages values are measured in 30-s time slots. The hardware platform

TABLE III
AVERAGED RESULTS FOR THE TEST DATA SETS (MEAN AND STANDARD DEVIATION) BEFORE AND AFTER OPTIMIZATION FOR ELBOW FLEXION AND EXTENSION (EF, EE) AND WRIST FLEXION AND EXTENSION (WF, WE)

		E_{rms} [Nm]	E_{max} [Nm]	ρ	η_4	η_6
Non optimized	ef	8.1 ± 2.2	15.3 ± 3.9	0.8 ± 0.1	0.2 ± 0.2	0.4 ± 0.2
	ee	9.1 ± 2.3	15.9 ± 4.9	0.84 ± 0.10	0.24 ± 0.16	0.40 ± 0.18
	wf	0.40 ± 0.1	0.85 ± 0.15	0.86 ± 0.03	0.64 ± 0.28	0.85 ± 0.16
	we	1.53 ± 0.52	2.85 ± 0.92	0.70 ± 0.05	0.16 ± 0.10	0.24 ± 0.13
Optimized	ef	4.2 ± 0.97	11.0 ± 3.0	0.87 ± 0.05	0.67 ± 0.11	0.85 ± 0.09
	ee	3.4 ± 1.3	9.6 ± 4.1	0.89 ± 0.08	0.79 ± 0.15	0.91 ± 0.09
	wf	0.26 ± 0.17	0.64 ± 0.24	0.80 ± 0.05	0.83 ± 0.26	0.92 ± 0.14
	we	0.39 ± 0.16	0.75 ± 0.25	0.42 ± 0.46	0.63 ± 0.28	0.82 ± 0.21

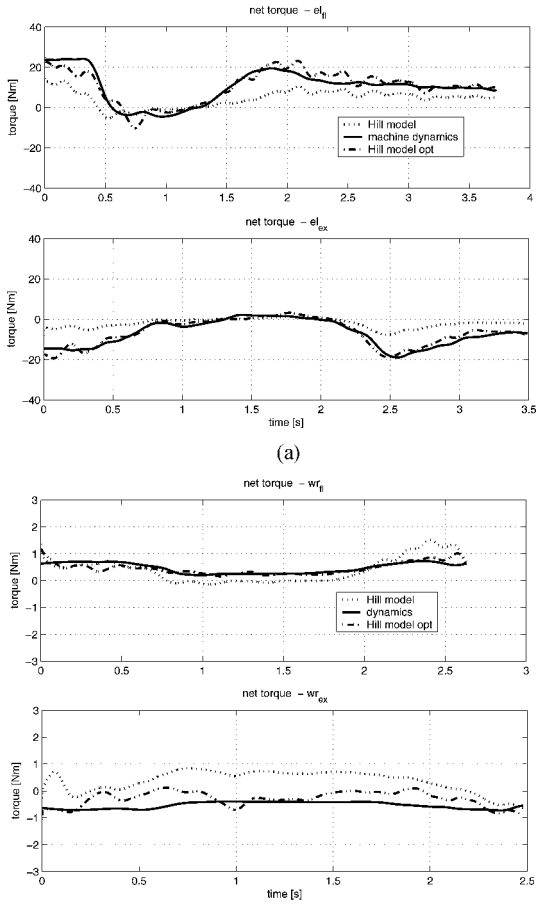

Fig. 8. Example of torques at the elbow during flexion (top – a) and extension (bottom – a). Torques at the wrist during flexion (top – b) and extension (bottom – b).

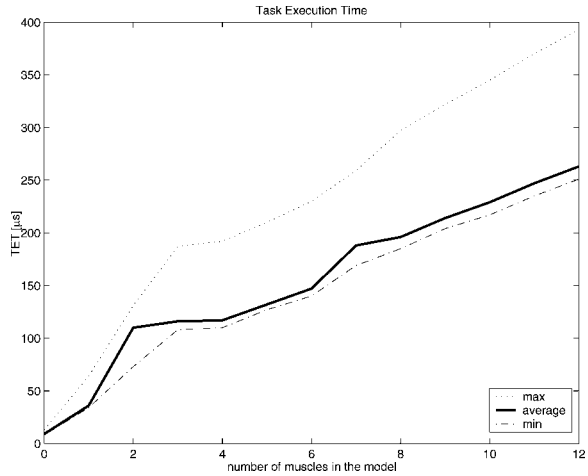

Fig. 9. Task Execution Time as a function of the number of myoprocessors (i.e., muscles that have been modelled).

was a PC104 with an Intel Pentium4@2.4 GHz processor and 512 Mb RAM. Nonlinearity of the TET as a function of muscle number can be observed, as a results of the different complexity of myoprocessors modeling different muscle.

IV. DISCUSSION

The main objective of this paper is to present the development, optimization, and integration of real-time myoprocessors as a HMI for an upper limb powered exoskeleton. As a key element of a neural controlled exoskeleton, the myoprocessors should be robust, providing accurate joint torque predictions over a broad range of loading and motion conditions.

Both black-box and white-box approaches were previously used for muscle modeling [6], [13], [15]. This study adopted an approach in which most of the internal parameters of the myoprocessor are directly related to physiological muscle parameters. More specifically, the core of the myoprocessor is a Hill-based muscle model together with a three-dimensional anatomical representation of the upper limb based on [23]–[25] and a nonlinear sEMG-to-Activation signal processor. At the same time, GAs are used to optimize the myoprocessor's internal parameters, for each specific subject wearing the exoskeleton, without the need for *a priori* exact knowledge of each muscle parameter. The optimization is constrained (as described in Section II-C) in order to prevent parameters from exceeding physiological ranges. In the authors' opinion, the resulting model has more characteristics in common with white-box models than with black-box models (e.g., neural networks), even if the adherence to physiology of the model can be improved at several levels: some elements, such as muscle pennation, can be included in the model structure; the optimization boundaries for each parameter can be different for each muscle in order to exploit all the knowledge available for the different muscles; the Hill model and the kinematic (skeletal) model can be optimized in an intertwined way (so

that, for example, a change in the origin or insertion point of a muscle, will be reflected in a corresponding change of tendon slack length and optimal fiber length).

As detailed in Section III, the parameter optimization has been carried out by using only a small dataset (4 recordings out of a total of 78 recordings). As indicated by the results, the ability of the myoprocessors to accurately predict the joint moment increased significantly with an optimized set of internal parameters. While optimization on a large set of data can yield better results during testing, it is also evident that, in general, it is not feasible to optimize the model on all the possible upper limb movements. Therefore, one of the goals of the current study was to verify that even with a relatively small database used for the optimization process, acceptable overall performances were achievable. This kind of robust performance is the main advantage of physiologically-based models over the black-box approach. In fact, if the physiologically based model captures the important features of the biological system, even using a small optimization database will yield a model that will then perform reasonably well in a broad range of conditions, although a specifically optimized model could outperform it in particular situations.

The myoprocessors' performance has been studied experimentally. For elbow movements, the results (see Table III) indicate that the integration of myoprocessors into a single neuromuscular model of the arm is capable of predicting the joint's torque with an average E_{rms} of about 8.6 Nm when parameters are not optimized. After optimization this prediction is improved to an average E_{rms} of 3.8 Nm. Moreover, after optimization, the percentage of time the absolute error stays below 4 Nm (η_4) is increased from an average 22% to an average 73%. Also for the wrist movements the E_{rms} is more than halved after optimization and η_4 shows an increase from 40% to 73%.

The predictions for the elbow joint movements showed better correlation (ρ) with the reference torques compared to the wrist joint. In particular wrist extension movements presented on average a lower ρ after the optimization, even when all the other error measures consistently improved. An explanation for this phenomenon can be provided by considering that finger flexors and extensors significantly contribute to the wrist flexion-extension torque [40], [41] but these muscles were not included in the model. In the case of the elbow joint, all the relevant muscles for the flexion-extension movement were included, which may explain the better ρ.

Given the synergistic behavior of the physiological muscles and the fact that some muscle were not accessible using noninvasive technique, the "maximum endurance of musculoskeletal function" criterion [31] has been used for predicting the contribution of the BRA muscle. One may note that this technique could be extended beyond its current use and could allow further reduction in the number of sEMG electrodes required for a satisfactory torque prediction.

In this study, particular attention has been devoted to the real time performances of the myoprocessors, so they can be integrated into the control system of the upper limb exoskeleton under development. Although all the myoprocessors share the same basic structure, they model muscles that are attached to the skeleton in different ways. Modeling more complicated cases in which the muscle wraps around several anatomical structures (multiple obstacles) requires more computational power than simpler conditions (single obstacle). By accounting for these constraints, myoprocessor complexity has been shaped to match the state of the art computational power. The resulting design allowed the 12 myoprocessors implemented to run simultaneously in real time with a maximum TET below 400 μs (Fig. 9). It is anticipated that the system in its final configuration will include about 20 myoprocessors modeling muscles of wrist, elbow, and shoulder joints and it will be able to meet the real-time requirement of the exoskeleton main control loop (computational interval of 1000 μs).

In conclusion the myoprocessor described in the paper provides a good balance between complexity and performance. Along with GAs for the optimization of the internal parameters for a specific user, an ensemble of myoprocessors can be used to build an HMI that is sufficiently simple to operate in real-time conditions. Moreover, based on the results previously obtained by one of the authors [5], [6] with a simpler myoprocessor, this new HMI seems to offer a level of performance adequate for its integration into the control loop of an upper limb, 7 DOF, powered exoskeleton. The integration of the HMI into the exoskeleton system represents the necessary and preliminary step towards the evaluation of a HMI of this type for future use in conjunction with rehabilitation devices.

ACKNOWLEDGMENT

The authors wish to thank A. Campbel. As an intern working at the Biorobotics lab, University of Washington, he integrated part of the real-time data acquisition system and assisted in the data collections.

REFERENCES

[1] R. S. Mosher, "Force reflecting electrohydraulic servo manipulator," *Electro-Tech.*, Dec. 1960.

[2] B. Makinson, Research and Development Prototype for Machine Augmentation of Human Strength and Endurance, Hardiman i Project GE Company Schenectady, NY, 1971, Tech. Rep. S-71-106.

[3] T. J. Snyder and H. Kazerooni, "A novel material handling system," in *Proc. IEEE Int. Conf. Robotics and Automation*, Apr. 1996, pp. 1147–1152.

[4] H. Kazerooni, "The human amplifier technology at the University of California, Berkeley," *Robot. Auton. Syst.*, vol. 19, pp. 179–187, 1996.

[5] J. Rosen, M. Brand, M. Fuchs, and M. Arcan, "A myosignal-based powered exoskeleton system," *IEEE Trans. Syst., Man, Cybern. A, Syst. Humans*, vol. 31, no. 3, pp. 210–222, 2001.

[6] J. Rosen, M. B. Fuchs, and M. Arcan, "Performances of hill-type and neural network muscle models – towards a myosignal based exoskeleton," *Comput. Biomed. Res.*, vol. 32, no. 5, pp. 415–439, Oct. 1999.

[7] J. P. Donoghue, "Connecting cortex to machines: Recent advances in brain interfaces," *Nature Neuroscience (suppl.)*, vol. 5, pp. 1086–1088, Nov. 2002.

[8] R. W. Norman and P. V. Komi, "Electromechanical delay in skeletal muscle under normal movement conditions," *Acta Physiol. Scand.*, vol. 106, pp. 241–248, 1979.

[9] P. R. Cavanagh and P. V. Komi, "Electromechanical delay in human skeletal muscle under concentric and eccentric contractions," *Eur. J. Appl. Physiol.*, vol. 42, pp. 159–163, 1979.

[10] P. F. Vint, S. P. Mclean, and G. M. Harron, "Electromechanical delay in isometric actions initiated from nonresting levels," *Med. Sci. Sports Exercise*, vol. 33, pp. 978–983, 2001.

[11] G. I. Zahalak, "An overview of muscle modeling," in *Neural Prostheses*, R. B. Stein, P. Peckham, and D. B. Popovic, Eds. New York: Oxford Univ. Press, 1992.

[12] K. Manal and T. S. Buchanan, "A one-parameter neural activation to muscle model: Estimating isometric joint moments from electromyograms," *J. Biomech.*, vol. 36, pp. 1197–1202, 2003.
[13] D. G. Lloyd and T. F. Besier, "An emg driven musculoskeletal model to estimate muscle forces and knee joint moments *in vivo*," *J. Biomech.*, vol. 36, pp. 765–776, 2003.
[14] F. E. Zajac, "Muscles and tendons: Properties, models, scaling, and application to biomechanics and motor control," *Crit. Rev. Biomed. Eng.*, vol. 17, pp. 359–411, 1989.
[15] A. L. Hof and J. W. Van Den Berg, "EMG to force processing I: An electrical analogue of the hill muscle model," *J. Biomech.*, vol. 14, no. 11, pp. 747–758, 1981.
[16] J. M. Winters and L. Stark, "Estimated mechanical properties of synergistic muscles involved in movements of a variety of human joints," *J. Biomech.*, vol. 21, pp. 1027–1041, 1988.
[17] M. A. Lemay and P. Crago, "A dynamic model for simulating movements of the elbow, forearm and wrist," *J. Biomech.*, vol. 29, pp. 1319–1330, 1996.
[18] K. An, F. Hui, B. Morrey, R. Linscheid, and E. Chao, "Muscles across the elbow joint: A biomechanical analysis," *J. Biomech.*, vol. 14, no. 10, pp. 659–669, 1981.
[19] W. Murray, S. L. Delp, and T. S. Buchanan, "Variation of muscle moment arms with elbow and forearm position," *J. Biomech.*, vol. 28, pp. 513–525, 1995.
[20] G. T. Yamaguchi, A. G. U. Sawa, D. W. Moran, M. J. Fessler, and J. M. Winters, *Survey Hum. Musculotendon Actuator Parameters*, pp. 69–93, 1990.
[21] G. Loren, S. Shoemaker, T. Burkholder, M. Jacobson, J. Fridén, and R. L. Lieber, "Human wrist motors: Biomechanical design and application to tendon transfers," *J. Biomech.*, vol. 29, no. 3, pp. 331–342, 1996.
[22] I. W. Charlton and G. R. Johnson, "Application of spherical and cylindrical wrapping algorithms in a musculuskeletal model of the upper limb," *J. Biomech.*, vol. 34, pp. 1209–1216, 2001.
[23] B. A. Garner and M. G. Pandy, "A kinematic model of the upper limb based on the visible human project (vhp) image dataset," *Comput. Meth. Biomech. Biomed. Eng.*, vol. 2, pp. 107–124, 1999.
[24] ——, "Musculoskeletal model of the upper limb based on the visible human male dataset," *Comput. Meth. Biomech. Biomed. Eng.*, vol. 4, pp. 93–126, 2001.
[25] ——, "The obstacle-set method for representing muscle paths in musculoskeletal models," *Comput. Meth. Biomech. Biomed. Eng.*, vol. 3, pp. 1–30, 2000.
[26] A. V. Hill, "The heat of shortening and the dynamic constants of muscle," in *Proc. Roy. Soc. Lond. Ser. B.*, 1938.
[27] D. R. Wilkie, "The mechanical properties of muscle," *Br. Med. Bull.*, 1956.
[28] J. M. Wilkie and D. R. Wilkie, "The dynamics of muscular contraction," *J. Physiol. (Lond.)*, 1958.
[29] J. M. Winters, "Hill based muscle models: A system engineering perspective," in *Multiple Muscle Systems: Biomechanics and Movement Organization*. New York: Springer-Verlag, 1990, pp. 69–93.
[30] O. Yarden, Dynamics of racket-arm interaction applied to tennis elbow Univ. Tel-Aviv. Tel Aviv, Israel, 1996, Ph.D. dissertation.
[31] R. D. Crowninshield and R. A. Brand, "A physiologically based criterion of muscle force prediction in locomotion," *J. Biomech.*, vol. 14, no. 11, pp. 793–801, 1981.
[32] P. Binding, A. Jinha, and W. Herzog, "Analytic analysis of the force sharing among synergistic muscles in one- and two-degree-of-freedom models," *J. Biomech.*, vol. 33, pp. 1423–1432, 2000.
[33] J. Holland, *Adaptation in Natural and Artificial Systems*. Ann Arbor, MI: Univ. Michigan Press, 1975.
[34] Z. Michalewicz, *Genetic Algorithms + Data Structures = Evolution Programs*, 3rd ed. Berlin, Germany: Springer-Verlag, 1996.
[35] C. R. Houk, J. A. Joines, and M. G. Kay, "A Genetic Algorithm for Function Optimization: A Matlab Implementation," Tech. Rep. North Carolina State Univ., 1995.
[36] R. Heine, K. Manal, and T. S. Buchana, "Using hill-type muscle models and emg data in a forward dynamic analysis of joint moment: Evaluation of critical parameters," *J. Mech. Med. Biol.*, vol. 3, no. 6, pp. 169–186, 2003.
[37] J. Basmajian and A. Blumenstien, *Eletrode Placement in EMG Biofeedback*. Baltimore, MD: William & Wilkins, 1980.
[38] J. F. Cram and G. S. Kasman, *Introduction to Surface Electromyography*. New York: Aspen, 1998.
[39] R. Chandler, C. CLauser, J. McConville, H. Reynolds, and J. Young, Investigation of Inertial Properties of the Human Body US Dept. Transportation, 1975, Tech. Rep. DOT HS-801 430.
[40] S. Delp, A. Grierson, and T. Buchanan, "Maximum isometric moments generated by the wrist muscles in flexion-extension and radial-ulnar deviation," *J. Biomech.*, vol. 29, no. 10, pp. 1371–1375, 1996.
[41] R. Gonzalez, T. Buchanan, and S. Delp, "How muscle architecture and moment arms affect wrist flexion-extension moments," *J. Biomech.*, vol. 30, no. 7, pp. 705–712, 1997.

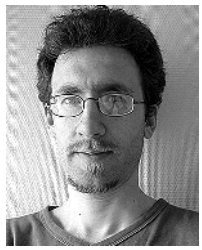

Ettore E. Cavallaro (S'05–M'06) received the Laurea degree in electric engineering (*magna cum laude*) from the University of Pisa, Pisa, Italy, in 2001, and the Ph.D. degree in bioengineering from Scuola Superiore Sant'Anna, Pisa, in 2006.

From 2001 to 2003 he was a Research Assistant at the Advanced Robotics Technology and Systems (ARTS) Lab of Scuola Superiore Sant'Anna. He currently works for a private company he co-founded. His research interests include: the study and development of prosthesis, neuroprosthesis and exoskeletons, with a particular emphasis on the Human-Machine Interface; the study and development of bio-inspired artificial sensors; the study of Soft Computing techniques (neural networks, fuzzy systems, and genetic algorithms) applied to biological signals processing.

Jacob Rosen (M'01) received the B.Sc. degree in mechanical engineering and the M.Sc. and Ph.D. degrees in biomedical engineering from Tel-Aviv University, Tel-Aviv, Israel, in 1987, 1993. and 1997. respectively.

From 1993 to 1997, he was a research associate developing and studying the myosignal based powered Exoskeleton at the Biomechanics Laboratory, Department of Biomedical Engineering, Tel-Aviv University. During the same period of time he held a biomechanical engineering position in a startup company developing innovative orthopedic spine/pelvis implants. Since 1997, he has been at the University of Washington, Seattle, currently as a Research Associate Professor of Electrical Engineering with adjunct positions in the Departments of Surgery and Mechanical Engineering. His research interests focus on surgical robotics, wearable robotics (Exoskeleton) biorobotics, biomechanics, and human-machine interface.

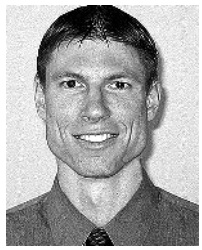

Joel C. Perry was born in 1978 in Bellingham, WA. He received the B.Sc. degree from Gonzaga University in 2000, and the M.Sc. and Ph.D. degrees from the University of Washington, Seattle, in 2002 and 2006, both in mechanical engineering.

From 2000 to 2002, he was a Research Assistant developing a powered prosthesis at the VA hospital, Seattle. Since 2002, he has been developing an anthropomorphic powered exoskeleton at the Biorobotics Laboratory, Department of Electrical Engineering, University of Washington. His research interests include medical device development, rehabilitation technologies for the disabled.

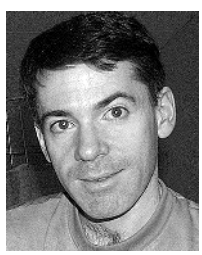

Stephen Burns received the Sc.B. degree in biology in 1988 and the M.D. degree in 1992, both from Brown University, Providence, RI.

From 1992 through 1996, he completed residency training in physical medicine and rehabilitation, first at the University of Washington. Seattle, and later at Thomas Jefferson University, Philadelphia, PA. Since 1996, he has provided patient care as a Staff Physician for the Spinal Cord Injury Center at VA Puget Sound Health Care System, Seattle. He is currently an Associate Professor in the Department of Rehabilitation Medicine at the University of Washington. His primary research interests focus on respiratory complications associated with spinal cord injury, motor recovery following traumatic tetraplegia, and wearable robotics.